Z. Kristallogr. **221** (2006) 186–197 / **DOI** 10.1524/zkri.2006.221.3.186

Effect of hydrostatic pressure on the crystal structure of sodium oxalate: X-ray diffraction study and *ab initio* simulations

Elena V. Boldyreva[*, I, II], Hans Ahsbahs[III], Vladimir V. Chernyshev[IV], Svetlana N. Ivashevskaya[I, V] and Artem R. Oganov[VI]

[I] Department of Solid State Chemistry, Research and Education Center «MDEST», Novosibirsk State University, Pirogova, 2, Novosibirsk, 90, 630090 Russia
[II] Institute of Solid State Chemistry and Mechanochemistry, Siberian Branch of the Russian Academy of Sciences, Kutateladze, 18, Novosibirsk, 128, 630128 Russia
[III] Philipps-Universitaet Marburg/Lahn, Hans-Meerwein Strasse, 35032 Marburg/Lahn, Germany
[IV] Chemistry Department, Moscow State University, 119899 Moscow
[V] Institute of Geology Karelian Scientific Center Russian Academy of Sciences, Pushkinskaya, 11, Petrozavodsk, 185610 Russia
[VI] Laboratory of Crystallography, Department of Materials ETH Hönggerberg, HCI G 515, Wolfgang-Pauli-Str. 10, 8093 Zurich, Switzerland

Received May 31, 2005; accepted July 25, 2005

Isosymmetric phase transition / Polymorphism / Density functional theory / Generalized gradient approximation / Powder diffraction structure analysis / X-ray diffraction / Sodium oxalate

Abstract. Effect of hydrostatic pressures up to 8 GPa on the crystals of $Na_2C_2O_4$ (sp. gr. $P2_1/c$) was studied in situ in the diamond anvil cells a) in neon, b) in methanol-ethanol mixture by high-resolution X-ray powder diffraction (synchrotron radiation, $\lambda = 0.7$ Å, MAR345-detector). Below 3.3–3.8 GPa, anisotropic structural distortion was observed, which was similar to, but not identical with that on cooling. At 3.8 GPa, a reversible isosymmetric first-order phase transition without hysteresis occurred. The orientation of the oxalate anions changed at the transition point by a jump, and so did the coordination of the sodium cations by oxygen atoms. *Ab initio* simulations based on the generalized gradient approximation of density functional theory have reproduced the main features of the structural changes in the crystals of sodium oxalate with increasing pressure. The theoretical pressure for the isosymmetric phase transition is 3.65 GPa, close to the experimental value; in agreement with experiment the transition was predicted to be reversible. *Ab initio* calculations gave a pronounced hysteresis for this transition, and have also predicted a further isosymmetric phase transition at 10.9 GPa, also with a hysteresis. The role of temperature in the pressure-induced phase transitions in sodium oxalate is discussed.

Introduction

Oxalates are widely used in the design of supramolecular structures with various desirable properties, and as precursors in solid-state chemical reactions. Therefore it is important to assess the sundry factors determining the crystal structures of oxalates and their response to external actions.

In general, in their crystalline forms oxalate-ions are usually considered as structure-forming units, defining the crystal packing (the framework) and the positions of other species, in particular of metal cations [1–3]. The variety of crystal structures arises because the sequence of alternating close packed layers formed by oxalate anions can differ: mono-layer (*AAA*), double-layer (*ABAB*), triple layer (*ABCABC*), etc. packings are known. Besides, non-spherical oxalate ions can rotate differently with respect to each other within the close packed layers and changing the angle between the plane of the oxalate ion and the close packed plane. Cations can occupy different positions within the framework formed by oxalate anions, so that their coordination polyhedra are different. Both "oxalate oxygen – metal cation" and "metal cation – metal cation" interactions account for the coordination of cations by oxalate ions "chosen" by a particular crystal structure [1–5].

Intermolecular interactions in crystalline oxalates are strong enough to modify the structure of the oxalate ion as compared with that optimized for this ion in the free state [5]. *Ab initio* calculations reported in several publications [5–8] have shown the free $(C_2O_4)^{2-}$ anion with torsion angle equal to 90° to be 0.274–0.294 eV/molecule lower in energy than a corresponding planar isomer. Staggered oxalate anions were recently observed in the structure of $Cs_2C_2O_4$ and in one of the two polymorphs of $Rb_2C_2O_4$ at ambient conditions [9], as well as in a few high-temperature polymorphs of $Rb_2C_2O_4$, $Cs_2C_2O_4$, $K_2C_2O_4$ [4]. However, according to the Cambridge Structural Database [10], in most crystal structures oxalate ions are essentially flat because of the electrostatic interactions between the carboxylate oxygens and metal cations in the crystal structures, and also because of the tendency of oxalate anions to form close-packed structures, for which the planar conformation of the oxalate ion is more favourable

* Correspondence author (e-mail: boldyrev@nsu.ru)

as compared with the twisted one [5, 8]. In ammonium oxalate, in hydrogen oxalates, in hydrates of oxalates, as well as in the crystalline oxalic acid the formation of hydrogen bonds between the species may be important for the conformation of oxalate ions and their crystal packing [1]. These hydrogen bonds are known to account not only for the structures, but also for crystal properties, *e.g.* the anisotropy of elastic properties or that of thermal expansion [11]. Structures of non-hydrated metal oxalates are of special importance in understanding the structure-determining factors in crystalline oxalates, since there are no hydrogen bonds, and their structures and general behaviour under various conditions are entirely determined by the interactions between oxalate anions and metal cations. These interactions are far from being "simple ionic" not only in oxalates of strongly chelating transition metals, or in silver oxalate with very strong Ag^+-Ag^+ attractive interactions, but even in the crystalline oxalates of alkali metals, such as sodium oxalate. This can be seen from the statistical analysis of polar hystograms showing the coordination of an oxalate oxygen atom in the structure by metal cations [5, 8]. Still, the structure-forming factors in alkali metal oxalates can be expected to be easier to understand, than those in the structures with more types of intermolecular interactions in the same structure. A very recent detailed study of a series of the anhydrous metal oxalates at variable temperature conditions has shown that a variety of phases exists, which are all related by subgroup-supergroup relations and can be described in a similar way [4]. Changes in the temperature and/or cation size result in the changes in the conformation of the oxalate-anions (staggered or flat), the deviation of the location of the centroids of the oxalate-anions from the ideal hexagonal packing, the ratio *c/a* of the more or less distorted hexagonal packing, and the coordination of metal cations by oxygen atoms in the voids of the packing [4].

We have initiated the studies of the effect of pressure on the structures of anhydrous metal oxalates. As the first system to study, we have chosen sodium oxalate, $Na_2C_2O_4$, as the easiest sample to handle. High pressure and low temperature were selected as the two methods of affecting the crystal structure. A pressure-induced phase transition into a previously unknown polymorph was observed at about 4 GPa by X-ray powder diffraction and by Raman spectroscopy. The results were preliminary discussed in [12, 13]. In the paper [12] we reported on the occurrence of a pressure-induced phase transition, but could not solve the high-pressure structure or even index the powder diffraction pattern obtained by a photographic technique using a laboratory X-ray source. In the paper [13] we have described briefly the results of structure solution of the high-pressure phase at 4.3 GPa. In the present contribution we give a more detailed description of the results of the experimental X-ray diffraction structural study of sodium oxalate on increasing pressure up to about 8 GPa and on subsequent decompression. The effect of hydrostatic pressure up to 15 GPa on the same system was simulated also *ab initio*. Theoretical predictions are in overall good agreement with experimental data.

Experimental

X-ray diffraction was first studied by a photographic method using MoK_{α_1} radiation ($\lambda = 0.7093$ Å) focused by a bent quartz crystal monochromator. Exposure time was 24 hours per measurement [12]. High pressure was created in a NBS Lever-Arm diamond anvil cell (DAC) [14]. Ethanol/methanol/water (16 : 3 : 1) mixture was used as a pressure-transmitting medium [15]. Ruby fluorescence technique [16, 17] was used for pressure measurements, with the accuracy of ± 0.05 GPa. Indexing of diffraction patterns was done based on the structural data for ambient pressure structure [18]. To avoid ambiguities in the indexing, pressure was increased very steadily, in small steps. The ratio of relative intensities of the reflections and a continuous character of changes in the interplane distances d_{hkl} with pressure was controlled. Lattice parameters were calculated from d_{hkl} using a program ULM [19].

After pressure reached 3.8 GPa, the X-ray powder patterns registered by the photographic method could no longer be indexed assuming a continuous distortion of the original phase, although positions of many lines were similar to those in the lower-pressure patterns. A reversible phase transition was assumed to take place, and the structure of the high-pressure polymorph was supposed to be related to that of the starting ambient pressure polymorph [12]. The powder diffraction patterns obtained by the photographic method did not allow us to find the reflection indices and to calculate cell parameters and volume (to say nothing of structure solution and refinement). Therefore we proceeded with a high-resolution X-ray difraction at a synchrotron radiation source ($\lambda = 0.7000$ Å) using a two-dimensional image plate MAR345 detector (pixel size 0.15 mm, 2300×2300 pixels in image, maximum resolution 1.105 Å, maximum 2θ 36.942 deg) for registration [13]. Experiments were run at BM1A at the Swiss-Norwegian Beamline at ESRF in Grenoble. The frames were measured with exposing time equal to 1200–3600 seconds, with $\Delta\varphi = 8$ degrees. The distance crystal – detector was adjusted using a Si-standard. The sample in the DAC was centered with respect to the beam very carefully, so that no reflections from steel gasket could be observed in the measured diffraction pattern.

Two types of diamond anvil cells were used in the high-resolution X-ray diffraction experiments: 1) a Merrill-Bassett cell of the four-screw type suggested by Mao and Bell [20, 21] modified by Ahsbahs [22], and 2) a cell without Be from one side, which avoids the absorption corrections for the powder-line intensities and allowed us to collect data without secondary Be-background from diamond reflections [23]. 220.0250/R/l steel was used as a gasket material. Two different pressure-transmitting media (neon and methanol/ethanol/water) were used, in order to check if pressure-transmitting medium has any effect on the phase transition. In general high-pressure phase transitions are known to be sensitive to the choice of a pressure-transmitting medium, even if there seems to be no direct chemical interaction between the medium and the solid sample [24].

The raw diffraction data were processed (calibration, masking, integration) using a Fit2D program [25]. The in-

dexing of the high-resolution powder diffraction pattern and the refinement of cell parameters and cell volume for the initial phase were straightforward, starting with the indices known for the ambient pressure structure. For the high-pressure phase, the unit cell dimensions were determined with the indexing program TREOR [26]. The structure solution and bond-restrained Rietveld refinements were performed with the MRIA program [27]. The strength of the restraints was a function of interatomic separation and for intramolecular bond lengths corresponded to an r.m.s. deviation of 0.03 Å. A special procedure of background subtraction [28] was applied to all measured patterns before refinement, resulting in patterns with almost linear background (compare the patterns in Fig. 1 and in Fig. 3 after and before background subtraction). All patterns were fitted using split-type pseudo-Voigt peak profile functions [29] and March-Dollase [30] texture correction with the [010] as a direction of preferred orientation. The structure of the high-pressure phase was first solved *ab initio*, without any preliminary assumptions on the structural model. Later, it was shown that it could be obtained also by refining the data starting from the atomic coordinates of sodium oxalate at ambient pressure.

Programs PCW [31], WebLabViewerLite [32], PLATON [33], and Mercury [34] were used to visualize the fragments of the crystal structure and to calculate selected geometric parameters. Program TENSOR by Y. Ohashi, published in [35], was used to calculate strain tensors [36] at different pressures. Voronoi polyhedra (VP) were calculated and visualized using VP_CIF [37].

Computational methodology

In the present work, we have used the ABINIT code [38], a common project of the Université Catholique de Louvain, Corning Incorporated, and other contributors (URL http://www.abinit.org), based on pseudopotentials and plane waves. It relies on an efficient Fast Fourier Transform algorithm [39] for the conversion of wavefunctions between real and reciprocal space, on the adaptation to a fixed potential of the band-by-band conjugate gradient method [40] and on a potential-based conjugate-gradient algorithm for the determination of the self-consistent potential [41].

The generalized gradient approximation [42] of density functional theory [43, 44] was used for the exchange-correlation. For an overview of density functional theory and the existing functionals, see [45]. The pseudopotentials used are of the Troullier-Martins [46] type, generated using the fhi98pp code [47] using the same GGA functional [42] as employed in present calculations. We used a very high kinetic energy plane-wave cut-off of 70 Ha and the Brillouin zone was sampled with a $4 \times 2 \times 1$ Monkhorst-Pack mesh [48]. These settings allowed us to achieve excellent convergence in pressure (within 0.02 GPa) and in the total energy (within 12 meV/atom). At each geometry, the ground state was found iteratively, until the maximum change in forces became smaller than 5×10^{-5} eV/Å. Structural optimisation was performed until the maximum forces were below 5×10^{-4} eV/Å and stresses were less than 0.003 GPa within the desired hydrostatic pressure values.

We started with the structure of the low-pressure phase, first optimised it at 0 GPa and then gradually increased pressure up to 15 GPa with steps of 1 GPa and then decompressed, from 15 GPa down to 1 GPa. It is well known that the GGA often gives accurate transition pressure values (see, *e.g.* [49–53]). Calculations similar to those reported here were able to predict an isosymmetric phase transition in sillimanite (Al_2SiO_5) under pressure [54]. However, simulations of molecular and ionic-molecular crystals (like those presented here) require much more attention to the performance of approximate density functionals for weak intermolecular bonds, and very careful structural optimisation (since the energy minima can be relatively flat).

Experimental results

X-ray powder diffraction patterns of sodium oxalate in the DAC filled with alcohol, or with neon at pressures below and above the transition point, as measured and after integration, can be obtained on request from the authors.

The results of the high-resolution X-ray powder diffraction experiments have confirmed qualitatively the conclusions, previously made from the photographic method measurements [12]: anisotropic continuous distortion of sodium oxalate was observed up to pressure equal to 3.3–3.8 GPa, after what a phase transition took place. We could not locate the transition pressure more exactly. The instability of pressure in the DAC at the phase transition point was also about 0.5 GPa. At the pressures close to the phase transition point the diffraction patterns clearly showed the presence of the two phases simultaneously: the original phase (continuous lines at the 2D powder diffraction patterns) and the high-pressure phase (spots, arcs). The increase in the relative content of the high-pressure phase with time at a constant pressure could be monitored. Thus, at 3.3 GPa the first reflections of the high-pressure phase were observed. We have measured a series of diffraction patterns at the same pressure at different time intervals. In about 12 hours the reflections of the low-pressure phase disappeared and there was only the high-pressure phase present in the sample. The transition was reversible, without any noticeable hysteresis within the accuracy of pressure measurement. The pressure-transmitting medium seemed to have no noticeable effect on the transition.

Independent optical microscopy observation of small (0.1 mm) single crystals of sodium oxalate in the DAC has shown that an interface formed in a crystal during a phase transition propagates very rapidly [13]. We can therefore suppose, that the two-phase systems at the phase transition region, which were observed in the case of powder samples, can be related to the difference in transition pressures for different crystallites (tiny crystals). For temperature-induced phase transitions, different transition temperatures for different crystals of various substances were reported previously [55–58]. Examples of different transition pressures for different samples were also reported. Thus, a

phase transition at 0.4 GPa was reported for pentaerythritol in [59], but no sign of it could be detected in another study even at 1.16 GPa [60]. No phase transitions were observed in single crystals of the monoclinic paracetamol I in the pentane-isopentane pressure-transmitting liquid at least up to 5 GPa [61], although a I → II transition took place in a powder sample in the same fluid at about 0.7−1.3 GPa [62].

The diffraction pattern of the high-pressure phase II could be indexed, and the cell parameters were refined. The plot showing the continuous change in the d_{hkl} values with pressure prior and after the phase transition point (thus proving the reliability and consistency of indicing), with the *hkl* indices assigned to every d_{hkl}-value in the two phases, can be obtained on request from the authors. With reflection indices found for the high-resolution diffraction patterns of the high-pressure phase of sodium oxalate, we could index also the previously obtained [12] films and refine cell parameters and cell volume for the high-pressure phase also from the data obtained by photographic method. *Ab initio* indexing of the same films failed because the first two reflections in the patterns were too weak and could not be observed with diffraction measured with a laboratory radiation source.

The structure of the high-pressure phase II could be successfully solved and refined in the $P2_1/c$ space symmetry group. Representative examples of Rietveld plots, showing the observed (after background correction) and difference profiles for sodium oxalate at ambient pressure, at 3.6 GPa (immediately prior to the phase transition), and at 4.3 GPa (immediately after the phase transition) are shown in Fig. 1. Parameters characterizing structure solution and refinement from powder diffraction data are summarized in Table 1[1].

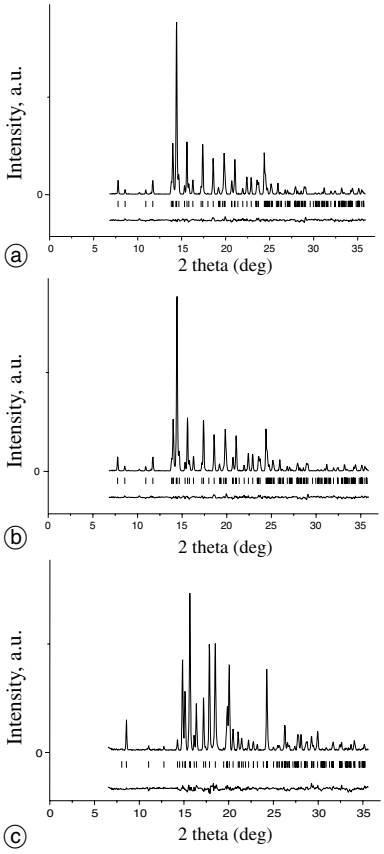

Fig. 1. The Rietveld plots, showing the observed (after background correction) and difference profiles for sodium oxalate: (**a**) at ambient pressure, (**b**) at 3.6 GPa, and (**c**) at 4.3 GPa.

Table 1. Parameters characterizing structure solution and refinement from powder diffraction data.

P, GPa	R_p	R_w	R_e
0.00[a]	0.1	0.110	0.37
1.05[a]	0.088	0.094	0.215
1.50[a]	0.087	0.094	0.199
1.90[a]	0.087	0.093	0.203
2.62	0.08	0.087	0.225
2.65[a]	0.104	0.108	0.243
3.26	0.098	0.1	0.224
3.34[a]	0.091	0.095	0.224
3.50	0.072	0.077	0.321
4.10	0.089	0.097	0.309
4.20[a]	0.124	0.141	0.342
4.54	0.078	0.084	0.3
5.99	0.076	0.079	0.284
7.12	0.075	0.079	0.291
7.97	0.102	0.12	0.291

a: The refinement was carried out for a system with neon.
R_p – '*R*-pattern': $R_p = \sum |Y_{obs} - Y_{calc}| / \sum |Y_{obs}|$
R_w – '*R*-weighted pattern': $R_w = (\sum w(Y_{obs} - Y_{calc})^2 / \sum wY_{obs}^2)^{1/2}$
R_{exp} – '*R*-expected': $R_{exp} = \sum \sigma(Y_{obs}) / \sum |Y_{obs}|$
Y_{obs} – the intensity in the *i*-th Bragg reflection,
Y_{calc} – the intensity assigned to the *i*-th Bragg reflection,
$\sigma(Y_e)$ – standard deviation of Y_{obs}.

Numbering of atoms in the following text is explained in Fig. 2. The values obtained for the samples in neon and in MeOH/EtOH mixture were similar. At ambient pressure, the results of the structure solution and refinement (general packing pattern, intermolecular angles and distances) for a sample in a DAC were in a good agreement with those previously reported from single-crystal X-ray diffraction experiments (Tables 2, 3) [8].

When pressure reached ∼8 GPa, a number of new weak reflections appeared in the diffraction pattern, nine of which (at 2θ: 11.61°, 15.95°, 16.86°, 17.52°, 19.13°, 20.04°, 23.39°, 24.82°, 25.45°) are shown on Fig. 3. All these peaks could be indexed in a monoclinic unit cell with acceptable dimensions and volume – $a = 3.36$ Å, $b = 5.25$ Å, $c = 9.20$ Å, $\beta = 88.6°$, $V = 162.2$ Å^3. On de-

[1] Full details on the refinement parameters at all the pressure values in the cells with different pressure-transmitting media, as well as the crystallographic data (cell parameters, atomic coordinates) have been deposited with the Cambridge Crystallographic Data Centre as supplementary publication no 265580–265593.
Numbering of atoms used in the CIFs is explained in Fig. 2.
Copies of available material can be obtained, free of charge via www.ccdc.cam.ac.uk/data_request/cif, by emailing data_request@ccdc.cam.ac.uk, or by contacting The Cambridge Crystallographic Data Centre, 12, Union Road, Cambridge CB2 1EZ, UK; fax: +44 1223 336033.
The list of F_o/F_c-data is available from the author up to five years after the publication has appeared.

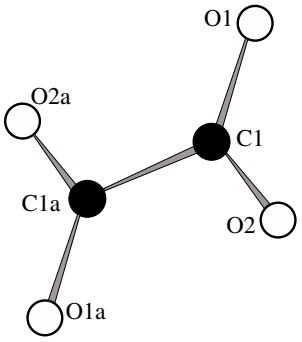

Fig. 2. An oxalate ion. Numbering of atoms is explained.

composition, these new lines slightly changed their positions and relative intensities, being indexable in the aforementioned monoclinic unit cell with the slightly increased volume. The origin of these new peaks requires further experimental studies. They can be related, in particular, to the formation of a new high-pressure phase, as predicted by *ab initio* calculation (see below).

The cell parameters and cell volume of sodium oxalate versus pressure below and above the transition point are plotted in Fig. 4. The data from the high-resolution powder technique obtained for the changes in a, c, β cell parameters and in the cell volume, V, versus pressure coincided well with the values calculated on the basis of the measurements by the photographic method [12]. Reliable results for cell parameter b could be obtained only with the higher precision of the high-resolution measurements.

Table 2. Cell parameters and volume of $Na_2C_2O_4$ at ambient conditions (experiment and *ab initio* simulations).

Parameter	single crystal data, 300 K[a]	powder diffraction data, 300 K	*ab initio* calculations, 0 K
a, Å	3.4847(6)	3.482(1)	3.556
b, Å	5.2639(6)	5.262(1)	5.286
c, Å	10.436(2)	10.432(2)	10.591
β, deg	93.08(2)	93.08(2)	93.84
V, Å^3	191.15(5)	190.86(8)	198.6

a: data from [8], deposited in CCDC, No 265760

Table 3. Fractional atomic coordinates in $Na_2C_2O_4$ at ambient conditions (experiment and *ab initio* simulations).

Atom	x	y	z
Na	0.3043(2)[a]	0.0572(2)	0.3547(1)
	0.309(2)[b]	0.058(1)	0.356(1)
	0.29845[c]	0.05652	0.35584
O1	0.1615(7)	−0.1206(4)	0.1510(2)
	0.159(4)	−0.127(2)	0.159(2)
	0.16121	−0.11676	0.15060
O2	0.2321(7)	0.2670(4)	0.0684(2)
	0.230(4)	0.276(3)	0.070(1)
	0.22946	0.26902	0.06707
C	0.1153(8)	0.0429(4)	0.0635(2)
	0.107(7)	0.037(5)	0.063(2)
	0.11343	0.04402	0.06311

a: single crystal data [8], CCDC No 265760
b: powder diffraction, this work,
c: *ab initio* simulations, this work

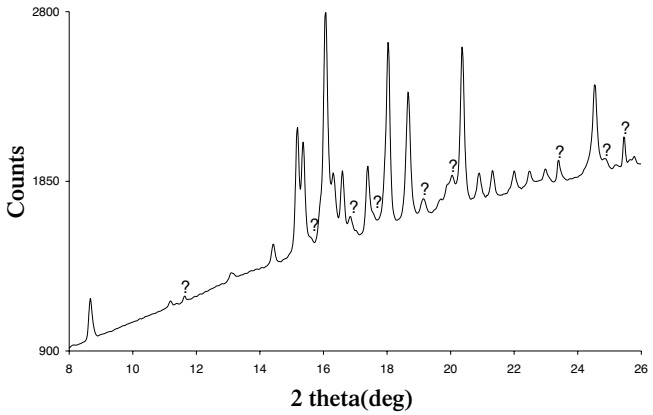

Fig. 3. A powder diffraction pattern (after integration) for the sample at about 8 GPa. The peaks that cannot be assigned to the phase II are marked (?).

Bulk compressibilities and deformation (strain) ellipsoids giving linear strain in selected crystallographic directions were calculated from the changes in cell parameters for the ambient-pressure polymorph prior to the phase transition, and for the high-pressure phase at pressures above 3.8 GPa (Fig. 5, Table 4). Bulk compressibility of the ambient-pressure polymorph was 1.6 times higher than that of the high-pressure phase: -8% GPa^{-1} and -5% GPa^{-1} respectively. Linear strain along the axes **1** and **2** (minimum compression and the direction normal to **1** and **3**) did not change much after the phase transition, whereas the maximum compression (linear strain along axis **3**) was noticeably (1.6 times) smaller in the high-pressure phase (-6% GPa^{-1} in the ambient-pressure polymorph and -4% GPa^{-1} in the high-pressure form). The orientation of the principal axes of the strain tensor with respect to the crystallographic axes changed slightly after the phase transition: the direction of the maximum compression (axis **3**) was almost preserved (rotated at about 10–15 degrees), remaining normal to the b axis, but the axes **1** and **2** interchanged.

For a comparison, we used the data on the crystal structure distortion of sodium oxalate on cooling down to 100 K [8, 12]. The data on the low-temperature structures of sodium oxalate obtained by Naumov, Boldyreva and Howard in 1996–1997 [8] remained unpublished, and were therefore deposited as CIFs at the CCDC now (Nos 265760 and 265761). The anisotropy of structural strain of the starting polymorph with increasing pressure was similar to, but not identical with that on cooling [12].

The crystal structure of sodium oxalate does not change its space-group symmetry $P2_1/c$ at the point of the phase transition, although the jumps in the pressure dependences of cell volume and cell parameters a, b, and β at the transition point were measured. So, the phase transition is an example of isosymmetric phase transitions, which were described previously also for other compounds [63–67]. Optical microscopy observations of a single crystal in the diamond anvil cell in the polarized light

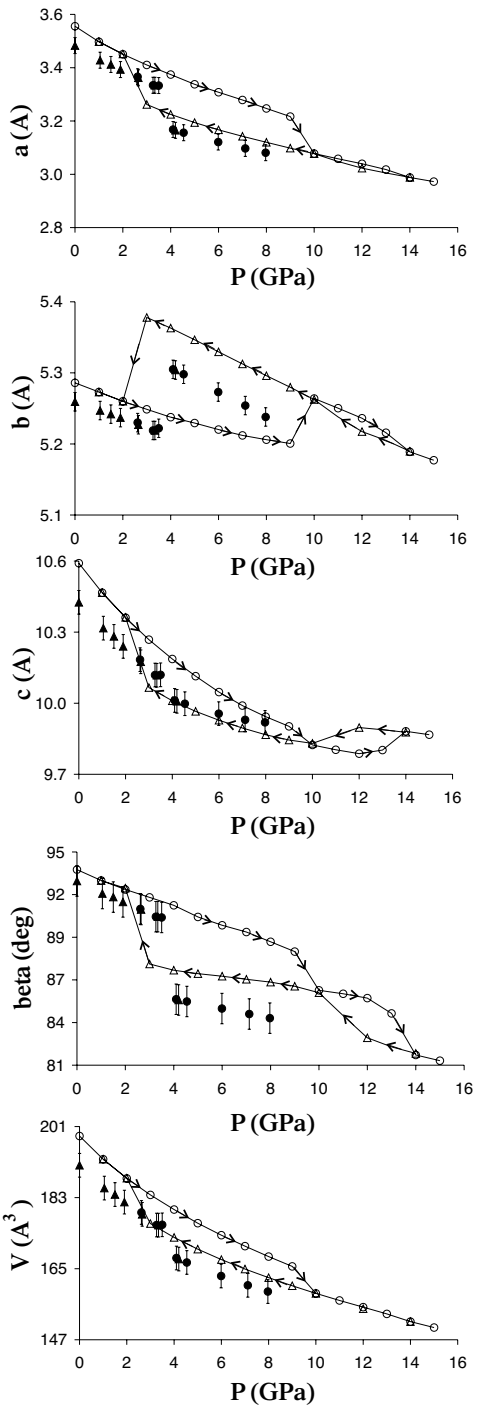

Fig. 4. Cell parameters and cell volume of sodium oxalate versus hydrostatic pressure. Black circles – DAC filled with methanol/ethanol/water mixture, pressure increasing; black triangles – DAC filled with Ne, pressure increasing. For a comparison, the results of the *ab initio* simulation are plotted at the same Figures: open circles – pressure increasing; open triangles – pressure decreasing.

[13, 68, 69] were in an agreement with the fact that the symmetry of the crystal did not change in the course of the phase transition. A peculiar feature of the pressure-induced structural change in sodium oxalate is that the monoclinic angle β decreases continuously from 93.08(2)° at ambient conditions to 90.75(1)° at 3.6 GPa right below the phase transition point, and then changes by a jump to 85.28(1)° at the phase transition point.

No changes in the intramolecular conformation of the oxalate anions with increasing pressure, also through the phase transition point could be noticed within the uncertainty. The oxalate-ions remained practically flat and centrosymmetric, the changes in the intramolecular OCO-angle and the torsion angle O2A–C1A–C1–O1 did not exceed 2 degrees. In this respect, the behaviour of sodium oxalate under pressure was very different from that of the oxalates of K, Rb, Cs with increasing temperature, where the changes in the conformation of the oxalate anions (staggered versus flat), known to be directly interrelated with the stability of an oxalate ion with respect to its decomposition [5], accompanied temperature-induced phase transitions [4, 9].

The main packing pattern did not change radically with increasing pressure. The centroids of the oxalate-ions formed a distorted pseudo-hexagonal packing (Fig. 6). The pseudo-hexagonal packing of the centroids of the oxalate ions can be visualized clearly also if Voronoi polyhedra (VP) are calculated. The VP for the centroids of oxalate ions immediately before and after the phase transition point are plotted in Fig. 7 [68].

The distortion of the pseudo-hexagonal packing could be characterized by the lengths and the angles of the pseudo-hexagonal mesh, the inclination of hexagonal planes formed by centroids of oxalate-anions with respect to the crystallographic $(b \times c)$ plane (angle ψ) and the ratios r_1/h, r_2/h, $r_{\text{aver}}/h (r_{\text{aver}} = (r_1 + r_2)/2)$, as was previously done for other metal oxalate structures [1, 4]. The r_{aver}/h ratio in the low-pressure polymorph of sodium oxalate at various pressures is in the range 1.59–1.64, that is close to the value 1.633 for the *c/a* ratio for the ideal close packing of spheres. The value of the ψ-angle in sodium oxalate is equal to zero, as in the ideal hexagonal packing. For different $Rb_2[C_2O_4]$ polymorphs the r_{aver}/h ratio is less than that for $Na_2[C_2O_4]$ (1.26–1.32 for γ, 1.24–1.25 for β, 1.27–1.31 for α) [4], and the value of the ψ-angle is not zero for some of them, that is the pseudo-hexagonal packing is more distorted, than that for sodium oxalate. With increasing pressure, the pseudo-hexagonal packing of the centroids of the oxalate ions in sodium oxalate becomes closer to the ideal one till the phase transition point is reached (the values of the α_1 and α_2 angles approach 120 degrees from different sides; the ratio r_{aver}/h approaches the value for the ideal packing 1.633). At the phase transition point, the values of r_{aver}/h, r_2, α_1 and α_2 change by a jump, whereas the value of r_1 decreases smoothly with pressure, also through the phase transition point. When pressure is increased further above the phase transition point, the values of α_1 and α_2 remain practically unchanged, r_2 decreases and r_{aver}/h increases. In general, the pseudo-hexagonal packing becomes more distorted with pressure increasing after the phase transition point (Fig. 6). For a comparison, using the variable-temperature data for sodium oxalate from [8], we have calculated r_1, r_2, r_{aver}/h, α_1 and α_2 at 100 K and at 295 K. The calculations at 295 K are in a good agreement with our data at ambient pressure: $r_1 = 5.844$ Å, $r_2 = 5.264$ Å, $r_{\text{aver}}/h = 1.594$ (295 K). On cooling down to 100 K the packing becomes slightly less distorted: r_{aver}/h becomes equal to

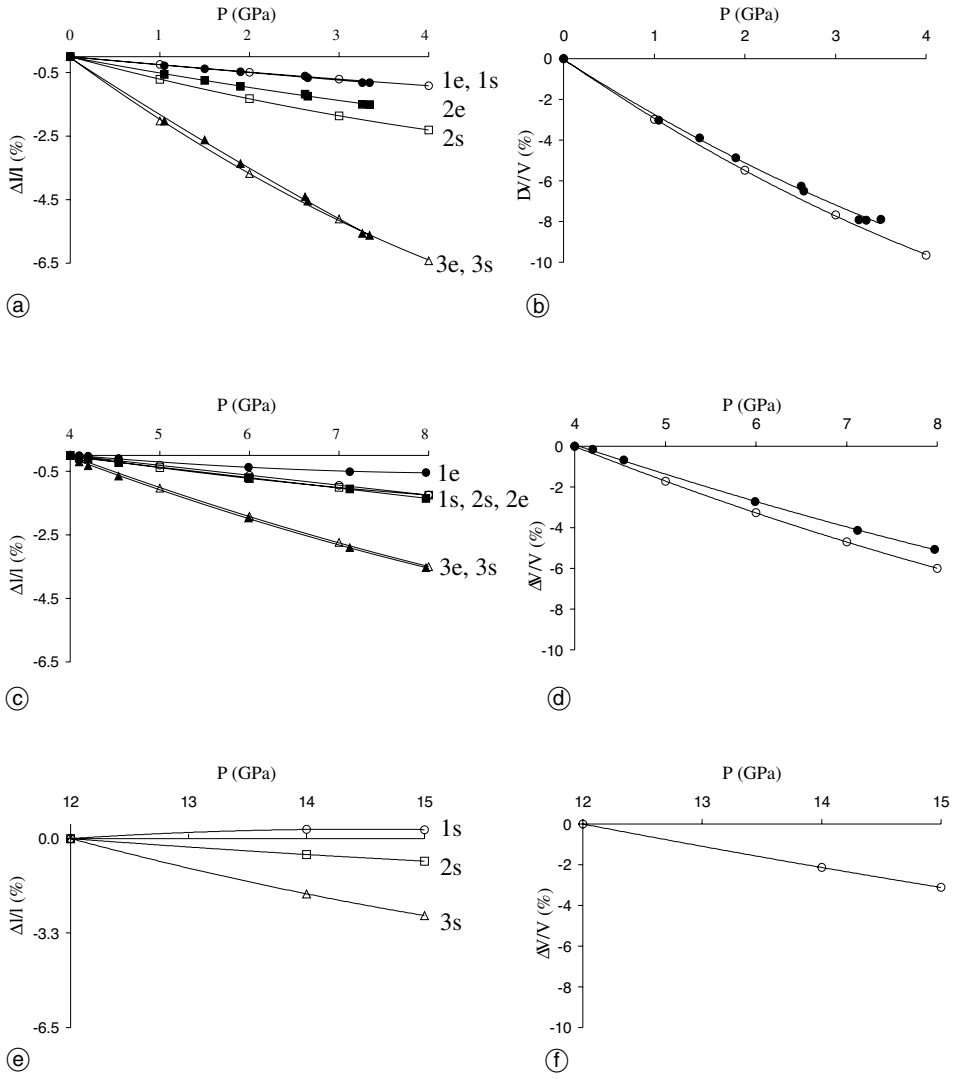

Fig. 5. Linear strain in the directions of the three principal axes (black circles – **1e**, black squares – **2e**, black triangles – **3e**) of the strain ellipsoids at pressures below (**a**) and above (**c**) the phase transition point at about 4 GPa. Bulk compressibility of the ambient-pressure polymorph I (**b**) and the high-pressure phase II (**d**). Orientations of the axes with respect to the crystal structure see in Table 4. For a comparison, linear strain and relative bulk changes versus pressure for the I (a, b), II (c, d), III (e, f) from the *ab initio* simulations are plotted: open symbols (**1s**, **2s**, **3s**).

1.604, and thus approaches the ideal value 1.633; the difference between $r_1 = 5.822$ Å, and $r_2 = 5.254$ Å becomes smaller at 100 K, than it was at 295 K. The values of α_1 and α_2 remained practically the same (within uncertainty) on cooling.

The major structural change at the phase transition point was related to a jumpwise rotation of the oxalate anions with respect to each other (Fig. 7). The values of the angles between the planes of the neighbouring oxalate ions (φ_1), and between the C−C axes of the two oxalate ions (φ_2) versus pressure are plotted in Fig. 8. The rotation of the anions is accompanied by an abrupt change in the coordination of the sodium cations by oxygen atoms at the phase transition point. This can be illustrated either by considering the pseudohexagonal packing, similarly to how this was done for the polymorphs of other metal oxalates [4] (Fig. 6), or by calculating the corresponding Voronoi polyhedra (Fig. 7). In the original polymorph, Na cations fill the distorted octahedral voids between the two anionic layers; coordination number of Na per O is equal to 6, if the two neighbours with Na−O distances >3 Å contributing small (solid angles less than 0.5 rad) faces to VP are neglected. In the high-pressure polymorph, the coordination number of Na is equal to 6, if only faces of VP

Table 4. Angles between the three principal axes of the strain ellipsoid and the crystallographic axes of sodium oxalate (degrees) at pressures below and above the phase (I–II) transition point (experiment and *ab initio* simulations).

	phase	Pressure, GPa	1×			2×			3×		
			a	*b*	*c*	*a*	*b*	*c*	*a*	*b*	*c*
exp	I	$P \leq 3.8$ GPa	90	0	90	55.4–56.1	90	37.0–37.6	33.9–34.6	90	127.0–127.6
	II	$P \geq 3.8$ GPa	60.3–63.2	90	22.2–25.2	90	0	90	26.8–29.7	90	112.2–115.2
calc	I	1–9	90	0	90	57.5–57.9	90	36.4–37.5	32.5–33.7	90	126.4–127.5
	II	9–13	65.6–70.6	90	16.7–21.7	90	0	90	19.4–24.5	90	106.7–111.7
	III	12–15	55.2–55.7	90	27.1–27.6	90	0	90	34.3–34.8	90	117.1–117.6

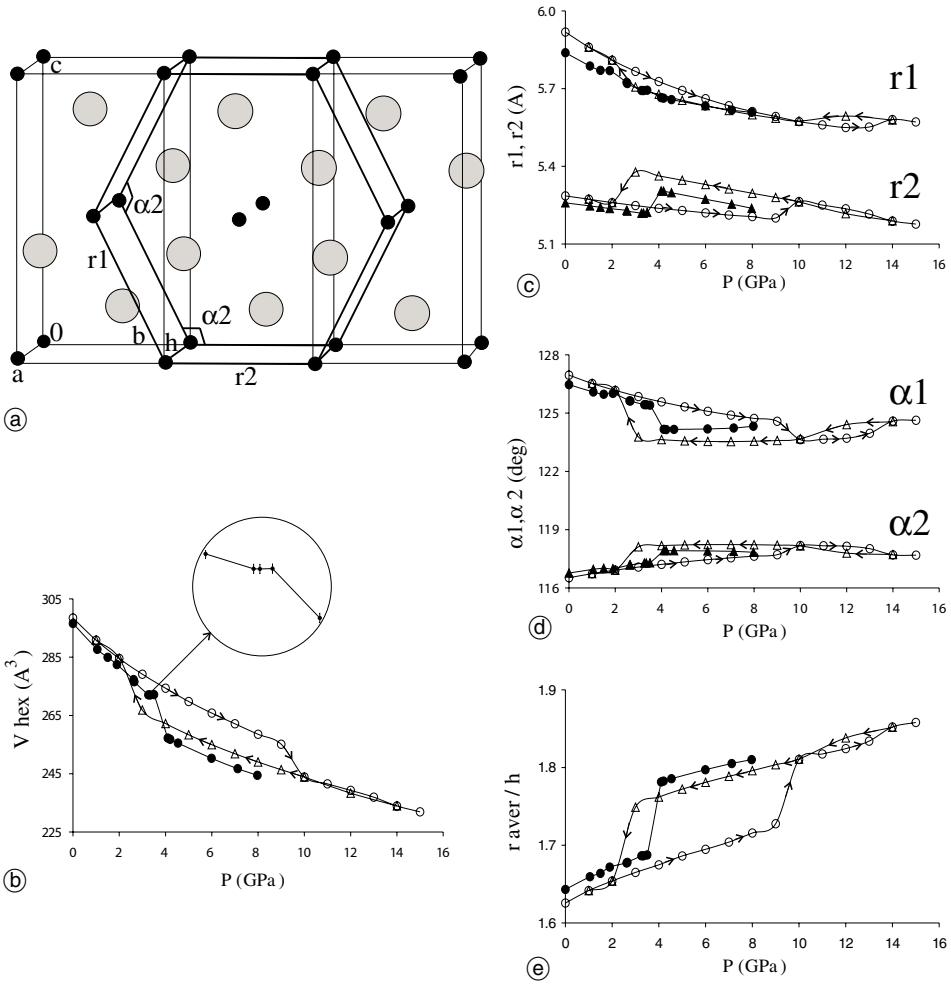

Fig. 6. (**a**) – The structure of sodium oxalate in a pseudo-hexagonal representation (as in [1, 4]). The center-of-gravity locations of the oxalate anions (small black balls) and the positions of Na cations (large grey balls) are drawn. The changes in the geometric parameters characterizing the mesh (**c**–**e**) and in the volume of a pseudo-hexagonal prism (**b**) versus pressure are plotted for a comparison, the results of the *ab initio* simulation are shown at the same plots: open circles – pressure increasing; open triangles – pressure decreasing.

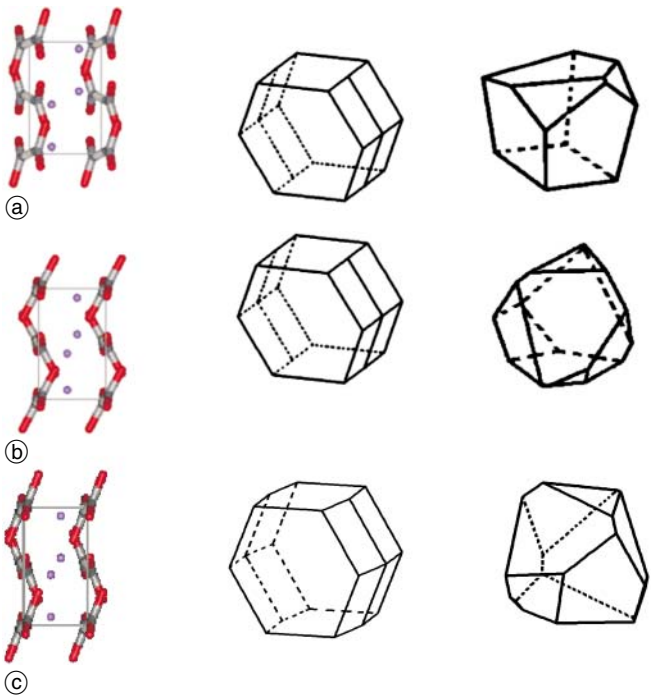

Fig. 7. From left to right: fragments of the crystal structure of sodium oxalate ((**b** × **a**) – projection), Voronoi polyhedra calculated for the centroids of oxalate anions and for the coordination of sodium cations by oxygen atoms; (**a**) before the phase transition; (**b**) after the phase transition; (**c**) for a comparison, the data for the phase III obtained in the *ab initio* simulations.

with solid angles larger than 1 rad (Na−O distance shorter than 3 Å) are taken into account; it increases and becomes equal to 7, if only faces of VP with solid angles larger than 0.6 rad are considered, and to 11 ($6 + 1 + 2 + 2$), if no faces (and, correspondingly, no neighbours) are neglected (Fig. 7). The sphericity coefficient [37] of a VP calculated for the coordination of Na by O increased from 0.56 to 0.61 on pressure-induced phase transition. 6 oxygen atoms in the coordination of a sodium ion can be related to the corresponding neighbours in the low-pressure structure. These 6 Na−O distances, as well as selected Na−Na distances are plotted versus pressure in Fig. 9. After the phase transition point, the Na-Na distances become more equal with each other, the average Na−Na distance decreasing. At the same time, one of the Na−O distances increases very noticeably as compared to its previous value and to the values of other Na−O distances at the same pressure. At the phase transition point, the Na-ions seem to be "pushed" further out of the planes formed by the pseudo-hexagonal packing of the oxalate anions (Figs. 7, 9).

Ab initio simulations

At $P = 0$ GPa, the agreement between theoretical and experimental crystal structures is rather good (Tables 2, 3), the main difference being that theory overestimates lattice

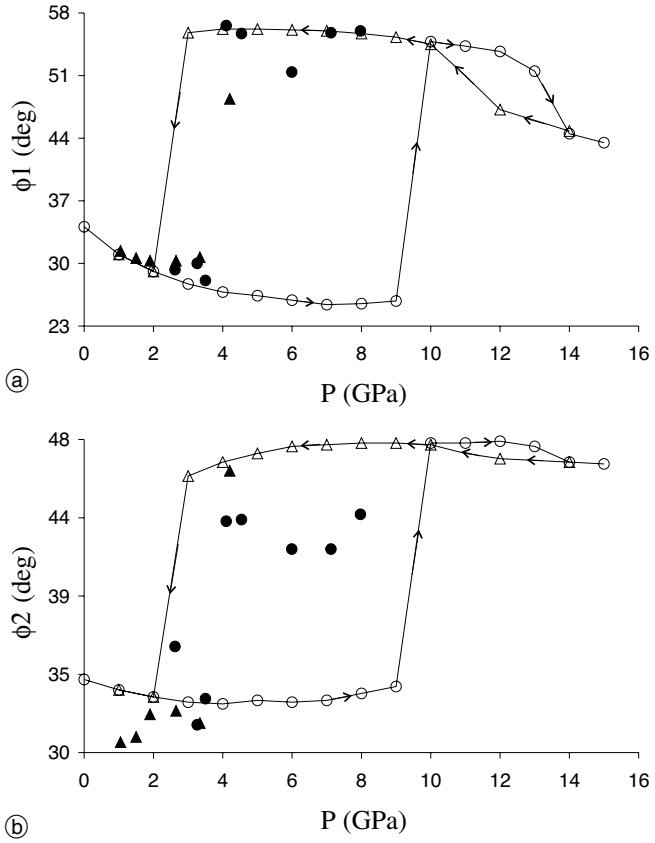

Fig. 8. Angles between the planes of the neighbouring oxalate ions (**a**), and between the C−C bonds of the neighbouring oxalate ions (**b**) in the structure of sodium oxalate versus hydrostatic pressure. Black triangles – DAC filled with Ne, black circles – DAC filled with methanol/ethanol/water mixture. For a comparison, the results of the *ab initio* simulation are plotted at the same Figures: open circles – pressure increasing; open triangles – pressure decreasing.

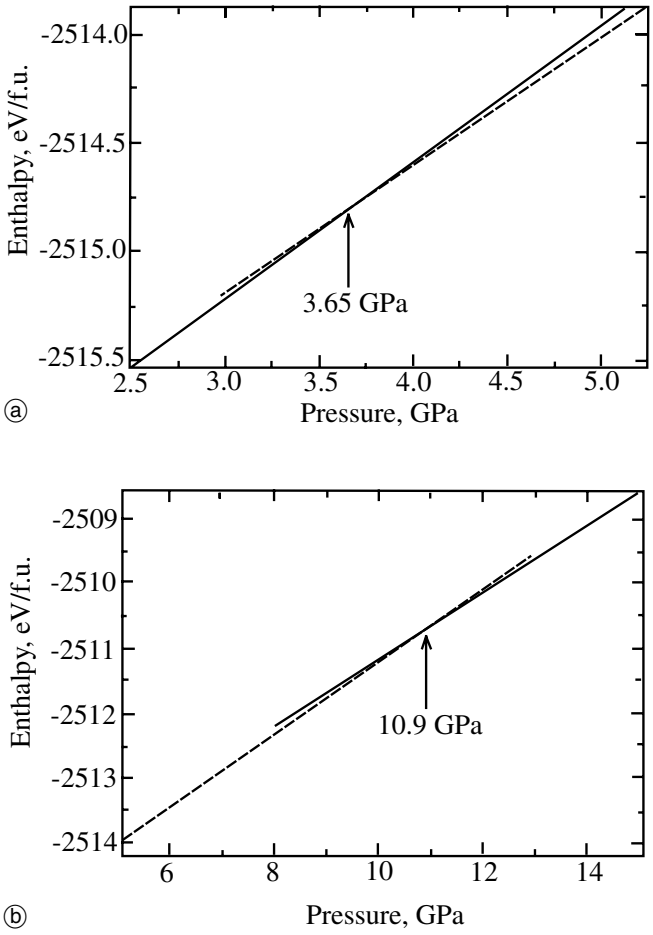

Fig. 10. Enthalpy *vs* pressure plots showing phase transitions at 3.65 GPa and 10.9 GPa.

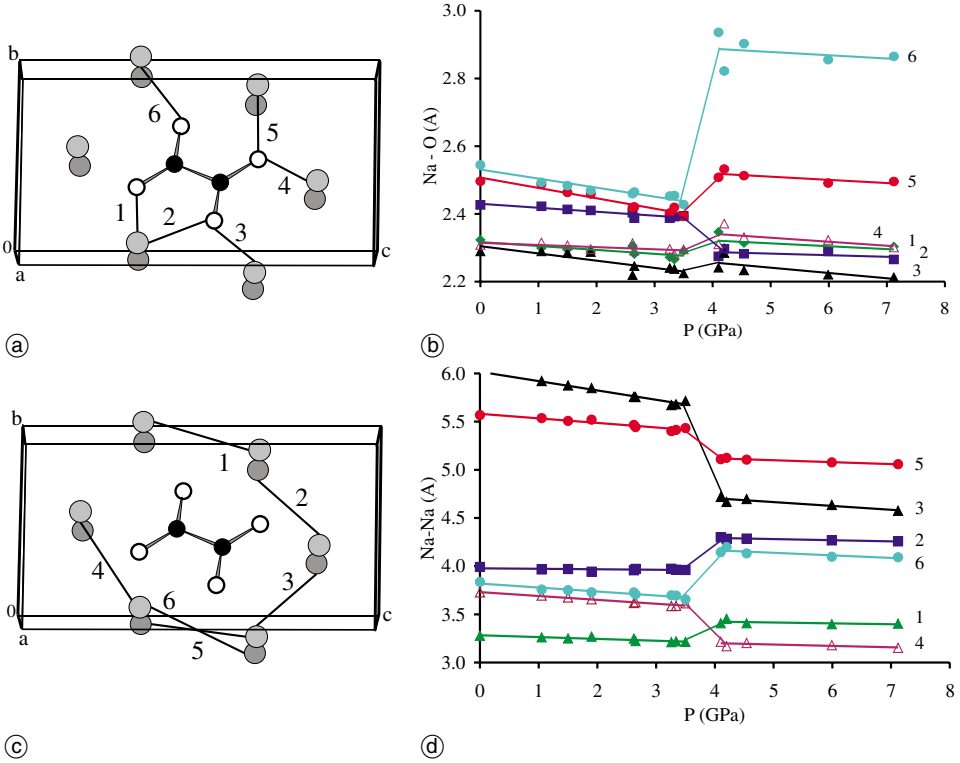

Fig. 9. Numeration of the selected Na−O (**a**) and Na−Na (**c**) distances in the structure of sodium oxalate and the changes in the corresponding distances versus pressure (**b**, **d**). In (**a**, **c**) black circles – carbon, open circles – oxygen. Light and dark grey circles – sodium atoms that are related by translation along **a**. Lines are guides to the eye.

parameters by ∼1%. This is typical of the GGA [45, 49, 50]. On increasing pressure simulations have resulted in an isosymmetric phase transition I → II with a discontinuous change in the orientation of the oxalate anions with respect to each other, and in the coordination of Na cations by oxygen atoms, which is also in an agreement with experimental data. The equilibrium phase transition pressure was estimated from the calculated *H(P)* curves (Fig. 10). The theoretical value (3.65 GPa) is in excellent agreement with the experimental value of 3.3–3.8 GPa. The simulated transition I → II was reversible, but, in contrast to the experimental data, characterized by a pronounced hysteresis (Fig. 4, 6, 8). On further compression, yet another isosymmetric phase transition (II → III), also with a hysteresis, was predicted by the simulations, the equilibrium pressure for it being equal to 10.9 GPa (Fig. 10). The transition manifested itself in the changes in cell parameters, in particular of the β angle (Fig. 4), and in the geometric parameters characterizing mutual orientation of the oxalate anions (Fig. 8). The main packing in the phase III resembled that in the phase I if viewed in the $(b \times c)$-projection, and that in the phase II – in the $(a \times c)$-projection (Fig. 11). Upon decompression, the low-pressure phase I was recovered at pressures around 2.5 GPa.

The bulk compressibility and the anisotropy of lattice strain of phases I and II obtained in the *ab initio* calculation were similar to the experimental values (Fig. 5, 6, Table 4). For the phase III predicted by calculations, but not (yet?) observed experimentally, the bulk compressibility and lattice strain were calculated and plotted for a comparison in the same Figures. The similarity in the crystal packing in the phases I, II, III may account for the small differences in the enthalpies of the three phases (Fig. 10).

The fact that simulations performed at zero Kelvin gave a pronounced hysteresis in contrast to what was observed experimentally has a straightforward explanation: in such simulations the forward/backward transitions are observed only when one of the structures no longer corresponds to an energy minimum and the energy barrier separating the two structures vanishes, and since minima corresponding to the two structures disappear at different pressures, there must be a hysteresis. When thermal vibrations are present, the transition will occur sooner: disappearance of the barrier is no longer needed, and transitions will occur once the barrier heights become comparable to the energy of thermal vibrations. At sufficiently high temperature the hysteresis may disappear completely: in the case of $Na_2C_2O_4$ at 300 K experiment did not detect any hysteresis, which means that the barrier for the transition is comparable to or lower than $k_B \cdot 300\ (\mathrm{K}) = 2.5$ kJ/mol. From general theoretical considerations a hysteresis must be expected at sufficiently low temperatures, and we expect that low-temperature experiments will reveal it for $Na_2C_2O_4$. The peculiarity of isosymmetric transitions is that they must be first-order (as is the case in $Na_2C_2O_4$), but can become fully continuous above a certain critical temperature [63]. At finite temperatures, domains of low- and high-pressure structures can coexist in the same

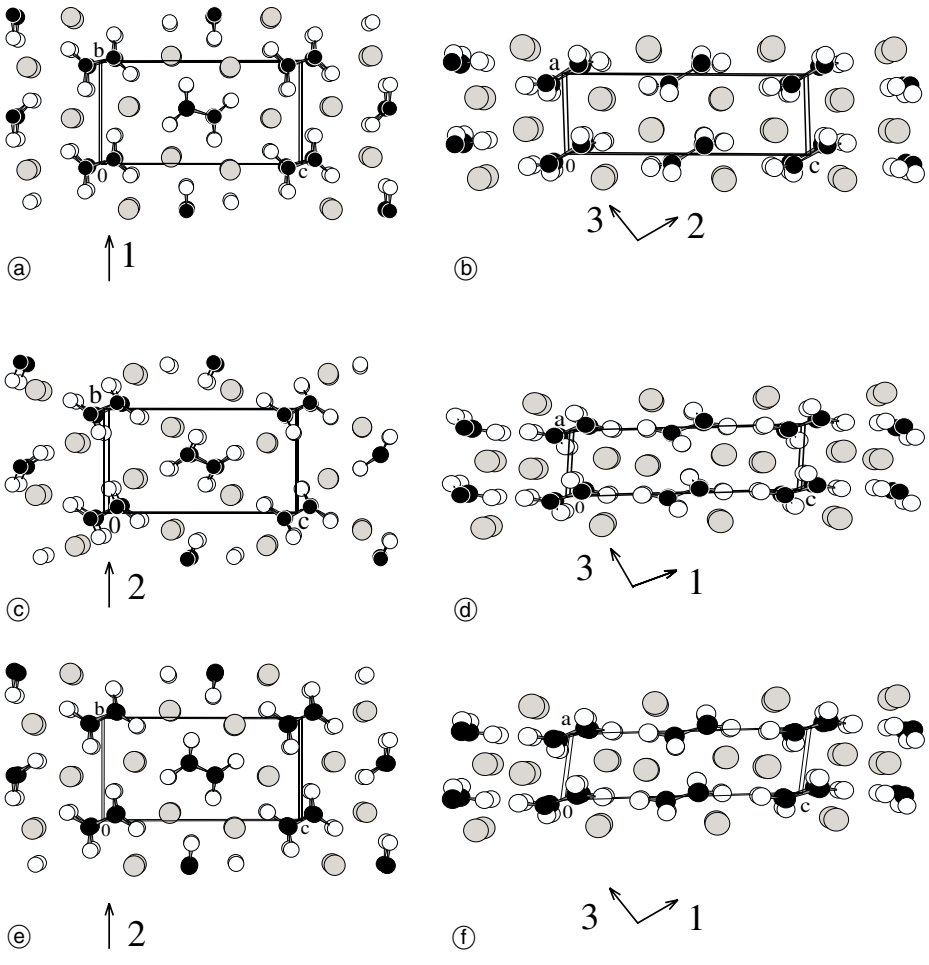

Fig. 11. Fragments of the crystal structure of sodium oxalate at 3.6 GPa (just before the phase transition) (**a**, **b**), at 4.3 GPa (immediately after the phase transition) (**c**, **d**) viewed along different axes. Orientation of the principal axes (**1**, **2**, **3**) of strain ellipsoid with respect to the crystal structure is shown (see also Table 1 and Fig. 4). For a comparison, the fragments of the phase III at the pressure of 15 GPa in the *ab initio* simulations are shown in the same projections (**e**, **f**).

phase; this is responsible for the decrease of the first-order character of these transitions with increasing temperature.

Conclusions

A reversible first-order isosymmetric phase transition takes place in the crystals of sodium oxalate at 3.3–3.8 GPa. Pressure results in the rotation of oxalate anions preserving to a large extent the main features of their packing, and a jump-wise change in the coordination of sodium cations by oxygen atoms at the transition point.

Experimental findings are confirmed by *ab initio* simulations. In particular, simulations find a reversible isosymmetric first-order transition with equilibrium pressure equal to 3.65 GPa, very close to the experimental transition pressure 3.3–3.8 GPa. At the same time, simulations predict some new phenomena for $Na_2C_2O_4$, not (yet?) observed experimentally: the existence of a second transition (II → III) at 10.9 GPa, and hysteresis in both transitions at sufficiently low temperatures. These predictions should stimulate new experiments. Recently, a combination of theory and experiment resulted in the discovery of a major Earth-forming mineral, a $CaIrO_3$-type phase of $MgSiO_3$ [52]. In this work, simulations also provide an evidence for yet another (possibly isosymmetric and not yet observed experimentally) high-pressure phase of sodium oxalate at 10.9 GPa, and this should be checked in future experimental work. A combination of low temperature and high pressure in the future experiments could also allow one to observe experimentally the hysteresis for the I → II and II → III phase transitions.

Acknowledgments. The authors acknowledge financial support of RFBR (grants 02-03-33358 and 05-03-32468), of the BRHE (a joint grant REC-008 of CRDF and Russian Ministry of Education NO-008-XI), the National Science Support Foundation for EVB (Program "Young Professors"), a CRDF grant Y2-CEP-08-07 supporting young scientists (SNI), grants 15384 (EVB) and 4222 (SNI) of Russian Ministry of Education. Diffraction experiments were supported by grant no 21-45703.95 from the Swiss National Science Foundation and the European Synchrotron Radiation Facility (ESRF), Grenoble (experiment HS-1239). Experimental assistance by the staff of the Swiss-Norwegian Beamlines at ESRF is gratefully acknowledged. ARO acknowledges financial support from ETH Zurich (grants TH-27033 and TH-32043). Calculations were performed at CSCS (Manno) and ETH Zurich.

References

[1] Naumov, D. Yu.; Podberezskaya, N. V.; Boldyreva, E. V.; Virovets, A. V.: Crystal structures of oxalic acid and its salts. Russian J. Struct. Chem. **37** (1996) 550–578.
[2] Kahn, O.: Bimetallic molecular-based magnetic materials. In: Molecular Magnetism: From Molecular Assemblies to the Devices (Eds. E. Coronado; P. Delhaes; D. Gatteschi; J. S. Miller). NATO ASI Series, Series E: Applied Sciences. Vol. 321, pp. 243–288. Kluwer: Dordrecht, 1996.
[3] Matyukha, V. A.; Matyukha, S. V.: Oxalates of rare-earth elements and actinides. Energoatomizdat, Moscow, 2004.
[4] Dinnebier, R. E.; Vensky, S.; Jansen, M.; Hanson, J.: Crystal structures and topological aspects of the high-temperature phases and decomposition products of the alkali-metal oxalates $M_2[C_2O_4]$ (M = K, Rb, Cs). Chem. Eur. J. **10** (2004) 1–12.
[5] Naumov, D. Yu.; Boldyreva, E. V.; Howard, J. A. K.; Podberezskaya, N. V.: The role of "ideal" and "real" crystal structure in the solid state decomposition of silver oxalate: experimental diffraction studies and theoretical calculations. Solid State Ionics **101–103** (1997) 1315–1320.
[6] Zhou, G.; Li, W.-K.: The abnormally long C−C bond in the oxalate ion. J. Chem. Educ. **66** (1989) 572.
[7] Dewar, M. J. S.; Zheng, Y.-J.: Structure of the oxalate ion. J. Molec. Struct. (Theochem) **209** (1990) 157–162.
[8] Naumov, D. Yu.: The application of structural analysis to the investigation of specific contacts in crystalline oxalates and their role in solid state decomposition. PhD. Thesis, Institute of Solid State Chemistry and Mechanochemistry, Siberian Branch of the Russian Academy of Sciences, Novosibirsk, Russia, 1997.
[9] Dinnebier, R. E.; Vensky, S.; Panthoefer, M.; Jansen, M.: Crystal and molecular structures of alkali oxalates: first proof of a staggered oxalate anion in the solid state. Inorg. Chem. **42** (2003) 1499–1507.
[10] Allen, F. H.: The Cambridge Structural Database: a quarter of a million crystal structures and rising. Acta Crystallogr. B**58** (2002) 380–388.
[11] Küppers, H.: Anisotropy of thermal expansion of ammonium and potassium oxalates. Z. Kristallogr. **140** (1974), 393–398.
[12] Boldyreva, E. V.; Shakhtshneider, T. P.; Ahsbahs, H.; Sowa, H.; Uchtmann, H.: Effect of pressure on the crystals of sodium oxalate: anisotropic structural distortion and a polymorphic transition. Russian J. Struct. Chem. **43** (2002) 107–113.
[13] Goryainov, S. V.; Boldyreva, E. V.; Smirnov, M. B.; Ahsbahs, H.; Chernyshev, V. V.; Weber, H.-P.: Isosymmetric reversible phase transition in sodium oxalate at 3.8 GPa. Doklady Physical Chemistry **390** (2003) 787–790.
[14] Weir, C. E.; Lippincott, E. R.; Van Valkenburg, A.; Bunting, E. N.: Infrared studies in the 1- to 15-micron region to 30000 atmospheres. J. Res. Natl. Bur. Stand. **63A** (1959) 55–62.
[15] Piermarini, G. J.; Block S.; Barnett, J. D.: Hydrostatic limits in liquids and solids to 100 kbar. J. Appl. Phys. **44** (1973) 5377–5382.
[16] Forman, R.A.; Piermarini, G. J.; Barnett, J. D.; Block, S.: Pressure measurement by utilization of ruby sharp-line luminescence. Science **176** (1972) 284–285.
[17] Piermarini, G. J.; Block, S.; Barnett, J. D.; Forman, R. A.: Calibration of the pressure dependence of the R_1 ruby fluorescence line to 195 kbar. J. Appl. Phys. **46** (1975) 2774–2780.
[18] Reed, D. A.; Olmstead, M. M.: Sodium oxalate structure refinement. Acta Crystallogr. B**37** (1981) 938-939.
[19] Brueggemann, R.; Mueller, B.; Debaerdemaeker, T.; Schmid, G.; Thewalt, U.: Computing program ULM for X-ray crystallography, University of Ulm (Germany), 1992.
[20] Merrill, L.; Bassett, W. A.: Miniature diamond anvil pressure cell for single-crystal X-ray diffraction studies. Rev. Sci. Instrum. **45** (1974) 290–294.
[21] Mao, K. H.; Bell, P. M.: Design and operation of a diamond-window high-pressure cell for the study of single crystal samples loaded cryogenically. Carnegie Inst. Yearbook **79** (1980) 409–411.
[22] Ahsbahs, H.: 20 Jahre Merrill-Bassett Zelle. Z. Kristallogr. Suppl. **9** (1995) 42.
[23] Ahsbahs, H.: New pressure cell for single-crystal X-ray investigations on diffractometers with area detectors. Z. Kristallogr. **219** (2004) 305–308.
[24] Boldyreva, E. V.; Ahsbahs, H.; Uchtmann, H.; Kashcheeva, N. E.: Effects of pressure on the two polymorphs of $[Co(NH_3)_5NO_2]I_2$: the anisotropy of lattice distortion and a phase transition. High Pressure Research **17** (2000) 79–99.
[25] Hammersley, A.: Fit2D, Version V11.012, hammersley@esrf.fr
[26] Werner, P.-E.; Eriksson, L.; Westdahl, M.: TREOR, a semi-exhaustive trial-and-error powder indexing program for all symmetries. J. Appl. Crystallogr. **18** (1985) 367–370.
[27] Zlokazov, V. B.; Chernyshev, V. V.: MRIA – a program for a full-profile analysis of powder multiphase neutron-diffraction time-of-flight (direct and Fourier) spectra. J. Appl. Crystallogr. **25** (1992) 447–451.
[28] Zlokazov, V. B.: DELPHI-based visual object-oriented programming for the analysis of experimental data in low energy physics. Nucl. Instr. Methods in Phys. Res. A**502**/2–3 (2003) 723–724.

[29] Toraya, H.: Whole-powder-pattern fitting without reference to a structural model: application to X-ray powder diffraction data. J. Appl. Crystallogr. **19** (1986) 440–447.
[30] Dollase, W. A.: Correction of intensities for preferred orientation in powder diffractometry: application of the March model. J. Appl. Crystallogr. **19** (1986) 267–272.
[31] Kraus, W.; Nolze, G.: PowderCell for Windows, Vers. 2.3, http://www.bam.de/a_v/v_1/powder/e_cell.html.
[32] WebLabViewerLite http://www.accelrys.com/about/overview/software.html
[33] Spek, A. L.: PLATON for Windows. University of Utrecht, The Netherlands, 2000.
[34] Bruno, I. J.; Cole, J.; Edgington, P. R.; Kessler, M.; Macrae, C. F.; McCabe, P.; Pearson, J.; Taylor, R.: New software for searching the Cambridge Structural Database and visualizing crystal structures. Acta Crystallogr. B**58** (2002) 389–397.
[35] Hazen, R.; Finger, L.: Comparative Crystal Chemistry. Temperature, Pressure, Composition and Variation of the Crystal Structure; Wiley: New York, 1982.
[36] Nye, J. F.: Physical Properties of Crystals; Their Representation by Tensors and Matrices. 3rd ed. Oxford Univ. Press, 1964.
[37] Medvedev, N. N.: Voronoi-Delonai polyhedra calculation for studying the crystalline and non-crystalline structures. OIGGM Publishing House, Novosibirsk, 2000, 213 pp.
[38] Gonze, X.; Beuken, J.-M.; Caracas, R.; Detraux, F.; Fuchs, M.; Rignanese, G.-M.; Sindic, L.; Verstraete, M.; Zerah, G.; Jollet, F.; Torrent, M.; Roy, A.; Mikami, M.; Ghosez, Ph.; Raty, J.-Y.; Allan, D. C.: First-principles computation of materials properties: the ABINIT software project. Comp. Mater. Sci. **25** (2002) 478–492.
[39] Goedecker, S.: Fast radix 2, 3, 4 and 5 kernels for Fast Fourier Transformations on computers with overlapping multiply-add instructions. SIAM J. Sci. Comput. **18** (1997) 1605–1611.
[40] Payne, M. C.; Teter, M. P.; Allan, D. C.; Arias, T. A.; Joannopoulos, J. D.: Iterative minimization techniques for *ab initio* total energy calculations: molecular dynamics and conjugate gradients. Rev. Mod. Phys. **64** (1992) 1045–1097.
[41] Gonze, X.: Towards a potential-based conjugate gradient algorithm for order-N self-consistent total energy calculations. Phys. Rev. B**54** (1996) 4383–4386.
[42] Perdew, J. P.; Burke, K.; Ernzerhof, M.: Generalized gradient approximation made simple. Phys. Rev. Lett. **77** (1996) 3865–3868.
[43] Hohenberg, P.; Kohn, W.: Inhomogeneous electron gas. Phys. Rev. **136** (1964) B864-B871.
[44] Kohn, W.; Sham, L. J.: Self-consistent equations including exchange and correlation effects. Phys. Rev. **140** (1965) A1133–A1138.
[45] Kurth, S.; Perdew, J. P.; Blaha, P.: Molecular and solid-state tests of density functional approximations: LSD, GGAs, and meta-GGAs. Int. J. Quant. Chem. **75** (1999) 889–909.
[46] Troullier, N.; Martins, J. L.: Efficient pseudopotentials for plane-wave calculations. Phys. Rev. B**43** (1991) 1993–2006.
[47] Fuchs, M.; Scheffler, M.: *Ab initio* pseudopotentials for electronic structure calculations of poly-atomic systems using density-functional theory. Comput. Phys. Commun. **119** (1999) 67–98.
[48] Monkhorst, H. J.; Pack, J. D.: Special points for Brillouin-zone integrations. Phys. Rev. B**13** (1976) 5188–5192.
[49] Zupan, A.; Blaha, P.; Schwarz, K.; Perdew, J. P.: Pressure-induced phase transitions in solid Si, SiO_2, and Fe: Performance of local-spin-density and generalized-gradient-approximation density functionals. Phys. Rev. B**58** (1998) 11266–11272.
[50] Oganov, A. R.; Brodholt, J. P.: High-pressure phases in the Al_2SiO_5 system and the problem of Al-phase in Earth's lower mantle: *ab initio* pseudopotential calculations. Phys. Chem. Minerals **27** (2000) 430–439.
[51] Oganov, A. R.; Gillan, M. J.; Price, G. D.: Structural stability of silica at high pressures and temperatures. Phys. Rev. B**71** (2005) art. 064104.
[52] Oganov, A. R.; Ono, S.: Theoretical and experimental evidence for a post-perovskite phase of $MgSiO_3$ in Earth's D″ layer. Nature **430** (2004) 445–448.
[53] Oganov, A. R.; Price, G. D.: *Ab initio* thermodynamics of $MgSiO_3$ perovskite at high pressures and temperatures. J. Chem. Phys. **122** (2005) art. 124501.
[54] Oganov, A. R.; Price, G. D.; Brodholt, J. P.: Theoretical investigation of metastable Al_2SiO_5 polymorphs. Acta Crystallogr. A**57** (2001) 548–557.
[55] Mnyukh, Yu.: Fundamentals of solid-state phase transitions, ferromagnetism, and ferroelectricity. 1st Books Library, 2001, 325 pp.
[56] Boldyreva, E. V.; Drebushchak, V. A.; Drebushchak, T. N.; Paukov, I. E.; Kovalevskaya, Yu. A.; Shutova, E. S.: Polymorphism of glycine: thermodynamic aspects. 1. Relative stability of the polymorphs. J. Therm. Analys. Calorim. **73** (2003) 409–418.
[57] Boldyreva, E. V.; Drebushchak, V. A.; Drebushchak, T. N.; Paukov, I. E.; Kovalevskaya, Yu. A.; Shutova, E. S.: Polymorphism of glycine: thermodynamic aspects. 2. Polymorphic transformations. J. Therm. Analys. Calorim. **73** (2003) 419–428.
[58] Boldyreva, E. V.; Drebushchak, V. A.; Paukov, I. E.; Kovalevskaya, Yu. A.; Drebushchak, T. N.: A comparative DSC and adiabatic calorimetry study of the monoclinic (I) and orthorhombic (II) polymorphs of paracetamol: an old problem revisited. J. Therm. Analys. Calorim. **77** (2004) 607–623.
[59] Frolov, A. P.; Vereshchagin, L. F.; Rodionov, K. P.: A study of the changes in cell parameters of pentaerythritol at pressures up to 10 000 kg/cm^2. Fiz. Tverd. Tela **4** (1962) 1608–1613.
[60] Katrusiak, A.: High-pressure X-ray diffraction study of pentaerythritol. Acta Crystallogr. B**51** (1995) 873–879.
[61] Boldyreva, E. V.; Shakhtshneider, T. P.; Vasilchenko, M. A.; Ahsbahs, H.; Uchtmann, H.: Anisotropic crystal structure distortion of the monoclinic polymorph of acetaminophen at high hydrostatic pressure. Acta Crystallogr. B**56** (2000) 299–309.
[62] Boldyreva, E. V.; Shakhtshneider, T. P.; Ahsbahs, H.; Sowa, H.; Uchtmann, H.: Effect of high pressure on the polymorphs of paracetamol. J. Therm. Analys. Calorim. **68** (2002) 437–452.
[63] Christy, A. G.: Isosymmetric structural phase transitions: phenomenology and examples. Acta Crystallogr. B**51** (1995) 753–757.
[64] Oganov, A. R.: Computer Simulation Studies of Minerals. University College London, 2002.
[65] Katrusiak, A.: High-pressure X-ray diffraction study on the structure and phase transition of 1,3-cyclohexanedione crystals. Acta Crystallogr. B**46** (1990) 246–256.
[66] Katrusiak, A.: Structure and phase transition of 1,3-cyclohexanedione crystals as a function of temperature. Acta Crystallogr. **B47** (1991) 398–404.
[67] Katrusiak, A.: Polymorphism of maleic hydrazide. Acta Crystallogr. B**57** (2001) 697–709.
[68] Boldyreva, E. V.: High-pressure induced structural changes in molecular crystals preserving the space group symmetry: anisotropic distortion/isosymmetric polymorphism, Cryst. Engineering **6**/4 (2004) 235–254.
[69] Boldyreva, E. V.; Drebushchak, T. N.; Shakhtshneider, T. P.; Sowa, H.; Ahsbahs, H.; Goryainov, S. V.; Ivashevskaya, S. N.; Kolesnik, E. N.; Drebushchak, V. A.; Burgina, E. B.: Variable-temperature and variable-pressure studies of small-molecule organic crystals, Arkivoc XII (2004) 128–155. (http://www.arkat-usa.org/ark/journal/2004/arkivoc articles 2004.asp).